INTERNATIONAL JOURNAL FOR NUMERICAL METHODS IN FLUIDS, VOL. 5, 13–23 (1985)

DEVELOPMENT AND APPLICATION OF AN ADAPTIVE FINITE ELEMENT METHOD TO REACTION–DIFFUSION EQUATIONS

J. I. RAMOS

Department of Mechanical Engineering, Carnegie-Mellon University, Pittsburgh, PA 15213, U.S.A.

SUMMARY

An adaptive finite element method is developed and applied to study the ozone decomposition laminar flame. The method uses a semidiscrete, linear Galerkin approximation in which the size of the elements is controlled by an integral which minimizes the changes in mesh spacing. The sizes and locations of the elements are controlled by the location and magnitude of the largest temperature gradient. The numerical results obtained with this adaptive finite element method are compared with those obtained using fixed-node finite-difference schemes and an adaptive finite-difference method. It is shown that the adaptive finite element method developed here using 36 elements can yield as accurate flame speeds as fourth-order accurate, fixed-node, finite-difference methods when 272 collocation points are employed in the calculations.

KEY WORDS Adaptive Finite Element Method Combustion

INTRODUCTION

The purpose of this paper is to develop an adaptive finite element method for reaction–diffusion equations. The method is also applied to study the ozone decomposition laminar flame. This flame has been the subject of numerous investigations. Of particular interest in this study are the works of Bledjian,[1] Margolis,[2] Meintjes,[3] Reitz[4] and Ramos.[5]

Bledjian[1] employed a second-order, fixed-node, method of lines technique and computed a flame speed of 54·3 cm/s using 100 grid points. Margolis[2] introduced an appropriate spline basis for the spatial variations, imposed collocation and boundary conditions and reduced the reaction–diffusion equations which govern the propagation of the ozone laminar flame in Lagrangian co-ordinates to a stiff initial value problem which was solved by standard techniques. Margolis used sixth-order B-splines and 272 collocation points and computed a flame speed of 49·7 cm/s. Meintjes[3] employed an explicit predictor–corrector method to study the same reaction–diffusion equations as Bledjian[1] and Margolis[2] and obtained a flame speed of 48 ± 2 cm/s when 121 grid points were employed in the calculations. The ± 2 cm/s error observed by Meintjes[3] was believed to be due to the calculation of the flame speed in real co-ordinates. This error could be minimized by calculating the flame speed in Lagrangian co-ordinates.

Reitz[4] employed a second-order, explicit, adaptive, Saul'yev[6] method and 30 grid points, and computed a flame speed of $49{\cdot}8 \pm 0{\cdot}1$ cm/s. This speed is in excellent agreement with that obtained by Margolis[2] who used a fourth-order accurate method. Ramos[5] developed a fourth-order accurate method of lines technique, a fourth-order accurate operator-splitting algorithm, three time-linearization algorithms, a moving finite element method, and an adaptive finite element

0271–2091/85/01 0013–11$01.10

Received 12 September 1983
Revised 6 February 1984

technique. The time-linearization schemes developed by Ramos[5] linearized the reaction terms in such a manner that the system of three reaction–diffusion equations which govern the ozone decomposition flame propagation is reduced to a system of uncoupled, linear equations which were solved by means of the standard tridiagonal matrix algorithm.[7] The first time-linearization algorithm developed by Ramos[5] was first-order accurate in time and second-order accurate in space; the second time-linearization algorithm was second-order accurate in both space and time; and the third time-linearization algorithm was second-order accurate in time and fourth-order accurate in space. The flame speeds computed with these three time-linearization schemes were 48·91 cm/s, 48·97 cm/s and 49·38 cm/s, respectively. These speeds were computed using 121 grid points.

The moving finite element method developed by Ramos[5] moves the grid according to the previously computed steady state flame speed but produces some errors because this speed is not steady at the beginning of the calculations. The steady state flame speed computed by Ramos[5] using the moving finite element method and 36 elements was 49·26 cm/s. In the adaptive finite element method, the elements were moved according to the location of the maximum temperature gradient. The adaptive finite element method with 36 elements produced a flame speed of 49·41 cm/s which compares very favourably with the speeds of 49·57 cm/s and 49·51 cm/s computed using 121 grid points with the fourth-order accurate method of lines and the fourth-order accurate operator-splitting technique developed by Ramos.[5]

In this paper, a new adaptive finite element method is developed and applied to study the ozone decomposition laminar flame. The method uses a linear, semidiscrete, Galerkin approximation in which the mesh spacing is minimized according to the location of the maximum temperature gradient. The method is based on some ideas developed by Reitz[4] for finite-difference schemes and employs a projection procedure for the calculation of the nodal amplitudes in the new grid. A similar projection method has also been used by Lee and Ramos[8] in their calculations of confined flame propagation problems. The results of the adaptive finite element method are compared with other numerical calculations which were performed with fixed-node finite-difference algorithms.

FORMULATION OF THE PROBLEM

We consider the propagation of a one-dimensional adiabatic flame through a combustible mixture of oxygen (O_2) and ozone (O_3). We assume that body forces are negligible, that the Mach number is small and that the species diffuse according to Fick's law with equal mass diffusivities for all of them. Under these assumptions, the equations governing the conservation of mass, momentum, energy and species reduce to

$$\partial\rho/\partial t + \partial(\rho u)/\partial x = 0 \tag{1}$$

$$p = p_0 = \text{constant} \tag{2}$$

$$\rho C_p[\partial T/\partial t + u\partial T/\partial x] = \partial(\lambda\partial T/\partial x)/\partial x - \sum_{i=1}^{3} h_i^0 w_i \tag{3}$$

$$\rho[\partial Y_i/\partial t + u\partial Y_i/\partial x] = \partial(\rho D\partial Y_i/\partial x)/\partial x + w_i, \quad i = 1,\ldots,N-1 \tag{4}$$

$$Y_N = 1 - \sum_{j=1}^{N-1} Y_i \tag{5}$$

$$\rho = p/\tilde{R}T \sum_{i=1}^{N} Y_i/W_i \tag{6}$$

where ρ is the density; $t(\geqslant 0)$ is the time; $x(-\infty < x < \infty)$ is the axial co-ordinate; u is the axial

velocity; p is the pressure ($p_0 = 0{\cdot}821$ atm); T is the temperature; C_p is the specific heat at constant pressure ($C_p = 0{\cdot}2524$ cal/g/K); λ is the thermal conductivity ($\lambda = 9{\cdot}112 \times 10^{-5}$ cal/cm/s/K); h_i^0 is the enthalpy of formation of species i; w_i is the reaction rate for species i; Y is the species mass fraction; N is the number of species; $\tilde{R}$ is the universal gas constant; and, W_i is the molecular weight of species i.

Equations (1), (3) and (4) can be reduced to a system of reaction–diffusion equations by introducing the mapping

$$(t, x) \rightarrow (t^*, \psi) \tag{7}$$

defined by

$$t^* = t;\ \partial\psi/\partial x = \rho;\ \partial\psi/\partial t = -\rho u \tag{8}$$

Introducing equations (7) and (8) into equations (2) and (4), assuming that the Lewis number is equal to 1 and $\alpha = \rho^2 D = \text{constant}$ ($\rho^2 D = 4{\cdot}3357813 \times 10^{-7}$ g^2/cm^4/s), we obtain

$$\partial T/\partial t^* = \alpha \partial^2 T/\partial \psi^2 - \sum_{i=1}^{N} h_i^0 w_i/\rho \tag{9}$$

$$\partial Y_i/\partial t^* = \alpha \partial^2 Y_i/\partial \psi^2 + w_i/\rho, \quad i = 1, \ldots, N-1 \tag{10}$$

In order to fully specify the problem we introduce the chemical reactions which govern the ozone decomposition. These reactions can be written as

$$O + O_2 + X \rightleftarrows O_3 + X \tag{11}$$

$$O + O_3 \rightleftarrows 2O_2 \tag{12}$$

$$O_2 + X \rightleftarrows 2O + X \tag{13}$$

where X represents a molecule of O, O_2 or O_3, and where the values of the reaction rates can be found, for example, in Reference 2. We only note here that the reaction rate terms, w_i, are highly non-linear functions of the temperature. We also define here Y_1 and Y_2 as the mass fractions of O_2 and O_3. Equations (9) and (10) were non-dimensionalized with $t_0 = 58{\cdot}78\ \mu$s, $\psi_0 = 5{\cdot}0478 \times 10^{-6}$ g/cm^2 and $T_0 = 300\ K$, where t_0 is a characteristic chemical time scale (there are in general a number of such scales due to the fact that there is a wide variation among the rates at which the different chemical reactions occur; the differential equations are therefore stiff), ψ_0 is a characteristic ψ-value defined as the product of the unburned gas density and a characteristic diffusion length (in our calculations, the characteristic diffusion length was defined as $(\rho_0 \lambda t_0/C_p)^{1/2}$ where ρ_0 is the unburned gas density) and T_0(= 300 K) is the unburned gas temperature. Note that for the ozone decomposition flame $N = 3$, and that equations (9) and (10) can be written in vector form as

$$\partial A/\partial t^* = a \partial^2 A/\partial \psi^2 + S \tag{14}$$

where

$$A^{\mathrm{T}} = (T, Y_1, Y_2) \tag{15}$$

$$S^{\mathrm{T}} = \left(-\sum_{i=1}^{3} h_i^0 w_i/\rho, w_1/\rho, w_2/\rho \right) \tag{16}$$

and the superscript T denotes transpose.

Equations (14), (15) and (16) were subjected to the following boundary and initial conditions

$$\partial A/\partial \psi(t, -\infty) = \partial A/\partial \psi(t, \infty) = 0 \tag{17}$$

$$A = \begin{pmatrix} 300 \\ 1/3 \\ 2/3 \end{pmatrix}, \quad 0 \leqslant \psi/\psi_0 \leqslant 8{\cdot}8 \tag{18}$$

$$A = \begin{pmatrix} 300 + 950\cos^5\left(\dfrac{\pi}{2}\dfrac{\psi_T - \psi}{1{\cdot}2\psi_0}\right) \\ 1/3 - 1/3\cos^5\left(\dfrac{\pi}{2}\dfrac{\psi_T - \psi}{1{\cdot}2\psi_0}\right) \\ 2/3 + (1/3 - 0{\cdot}0005)\cos^5\left(\dfrac{\pi}{2}\dfrac{\psi_T - \psi}{1{\cdot}2\psi_0}\right) \end{pmatrix}, \quad 8{\cdot}8 \leqslant \psi/\psi_0 \leqslant 10 \tag{19}$$

where $\psi_T = 50\psi_0 = 2{\cdot}5239 \times 10^{-4}\,\mathrm{g/cm^2}$, and where the domain $-\infty < \psi < \infty$ has been truncated to $0 \leqslant \psi \leqslant \psi_T$. The downstream location of the truncated domain corresponds to that of Ramos.[5] The initial conditions given by equations (18) and (19) were non-dimensionalized in exactly the same manner as equations (9) and (10). Equation (14) yields the values of T, Y_1 and Y_2. The value of Y_3 can be calculated from equation (5). The value of ρ can be calculated from the equation of state, i.e. equation (6). The value of x can be calculated from equation (8) as follows:

$$x = \int_{-\infty}^{\psi} \mathrm{d}\psi/\rho \tag{20}$$

which in the truncated domain can be written as

$$x = \int_{0}^{\psi} \mathrm{d}\psi/\rho, \quad 0 \leqslant \psi \leqslant \psi_T \tag{21}$$

For convenience we define a non-dimensional Cartesian co-ordinate X as

$$X = x\rho_0/\psi_0 = \int_{0}^{\psi} \mathrm{d}(\psi/\psi_0)/(\rho/\rho_0) \tag{22}$$

where ρ_0 is the density of the unburned gases ($\rho_0 = 1{\cdot}201 \times 10^{-3}\,\mathrm{g/cm^3}$) which are located at the upstream boundary.

Under steady state conditions one can define a steady state wave speed as follows

$$\partial Y_i/\partial t^* + U_i \partial Y_i/\partial\psi = 0, \quad i = 1, 2 \tag{23}$$

which when substituted into equation (10) yields, after integration,

$$U_i[Y_i(t^*, -\infty) - Y_i(t^*, \infty)] = \int_{-\infty}^{\infty} w_i\,\mathrm{d}\psi/\rho, \quad i = 1, 2 \tag{24}$$

Note that equation (24) yields two steady state flame speeds for Y_1 and Y_2. These speeds are the same in steady state.

ADAPTIVE FINITE ELEMENT FORMULATION

As we mentioned before the domain $-\infty < \psi < \infty$ was truncated to $0 \leqslant \psi \leqslant \psi_T$. We define $\psi_1 = 0$ and $\psi_{NE+1} = \psi_T$, where NE is the number of elements. If an equally-spaced grid is used in the calculations with mesh spacing h then $NE = (\psi_T - \psi_1)/h$. The ozone flame is characterized by the presence of very localized and steep temperature and concentration gradients. One would like to resolve these steep gradients very accurately because they correspond to the flame front where the

conversion of fuel and oxidizer to combustion products occurs. Evidently, one would like to concentrate the grid points where they are needed, i.e. at the flame front. Thus, unequally-spaced grids are desirable.

By analogy with the case of equally-spaced grids we define a function $h(\psi)$ which represents the grid spacing or size of the finite elements in such a manner that the total number of elements in $0 \leqslant \psi \leqslant \psi_T$ is fixed and equal to NE. We then have that

$$\mathrm{NE} = \int_0^{\psi_T} \mathrm{d}\psi / h(\psi) \tag{25}$$

is a constraint that must be satisfied. Note that if $h(\psi) =$ constant we obtain the expression that we derived before for an equally-spaced grid, i.e. $\mathrm{NE} = (\psi_T - \psi_1)/h$. Furthermore, we know that if the maximum temperature gradient is located at ψ_m, a measurement of the smallest grid spacing is

$$h_m = \left| \frac{\Delta T}{(\partial T/\partial \psi)_{\max}} \right| \tag{26}$$

where $\Delta T = T_b - T_u$ and T_b and T_u are the temperatures of the burned ($\psi = \psi_T$) and unburned ($\psi = 0$) gases, i.e. 1250 K and 300 K, respectively. In practice, the right-hand side of equation (25) can be multiplied by a constant (in the calculations reported here this constant is 4) which is related to the number of elements in the region of largest temperature gradient.

Equation (26) yields the value of the minimum grid spacing once the location of the largest temperature gradient is known. However, it does not yield any information about the location of other grid points. This information can be obtained by remembering that our objective is to resolve the flame front. Therefore, a large number of grid points should be placed there. This means that the grid spacing variations at the flame front (the grid spacing variations are defined as $\mathrm{d}h/\mathrm{d}\psi$, i.e. as the change in the size of the finite elements in space) should be minimized. This can be achieved by defining a functional which is related to the grid spacing variations. One such functional is

$$F(h) = \int_0^{\psi_T} \frac{\mathrm{d}\psi}{h} \left(\frac{\mathrm{d}h}{\mathrm{d}\psi} \right)^2 \tag{27}$$

The minimization of the functional defined of equation (27) will yield the grid spacing. However, this functional is subjected to the constraint given by equation (25), i.e. the number of elements is fixed. Introducing the Lagrange multiplier β and minimizing the functional $F(h)$ subjected to the constraint NE (equation (25)) one obtains the following differential equation

$$2h \frac{\mathrm{d}^2 h}{\mathrm{d}\psi^2} - \left(\frac{\mathrm{d}h}{\mathrm{d}\psi} \right)^2 - \beta = 0 \tag{28}$$

whose solution can be written as

$$h(\psi) = \frac{\beta}{4h_m} (\psi - \psi_m)^2 + h_m \tag{29}$$

Equation (29) has been obtained from the solution of equation (28) by requiring that the minimum element size be placed at ψ_m, i.e. at the location of the largest temperature gradient, and by requiring that $(\partial h/\partial \psi)_{\psi_m} = 0$. This condition means that the minimum grid spacing or the smallest finite element is located at the flame front.

Equation (29) could have been postulated as the grid spacing criterion. Other possible grid location techniques are, of course, possible as can be easily seen by defining other $F(h)$ functional (cf. equation (27)). Note that the grid spacing defined by equation (29) is based on the assumption

that the number of finite elements employed in the calculations is fixed, i.e. equation (25). Therefore, the adaptive technique developed here cannot be used in its present form in problems characterized by the presence of several moving steep gradient regions.

Substituting equation (29) into equation (25) and integrating, one can calculate the value of β as

$$\frac{\mathrm{NE}\sqrt{\beta}}{2} = \arctan\left(\frac{\psi - \psi_{\mathrm{m}}}{h_{\mathrm{m}}}\frac{\sqrt{\beta}}{2}\right)\Bigg|_{\psi=0}^{\psi=\psi_{\mathrm{T}}} \tag{30}$$

Equation (30) can also be used to calculate the location of the elements by replacing the value of NE by i and ψ_{T} by ψ_i where $i = 2, 3, \ldots, \mathrm{NE}$.

Note that the co-ordinates of the element nodes, ψ_i, depend on the location of the largest temperature gradient through equations (30) and (26). However, the locations of ψ_1 and $\psi_{\mathrm{NE}+1}$ were kept fixed and equal to 0 and ψ_{T}, respectively.

Equations (28) and (30) yield the locations of the grid points once the location of the largest temperature gradient is known. In unsteady flame propagation problems such as the one studied here, the location of the steepest temperature gradient varies with time. If we evaluate equations (26), (29) and (30) at each time step we would obtain an accurate but expensive numerical procedure. Numerical experiments suggest that it is very expensive to redefine a grid every time step and that substantial savings without much loss of accuracy can be achieved by defining a suitable criterion for grid redefinition. In the calculations reported here, the following procedure for grid redefinition was found accurate and inexpensive.

Suppose that ψ_{m}^n and h_{m}^n denote the location of the largest temperature gradient and the minimum nodal spacing at time t^n. Then, the mesh was only redefined if the new ψ_{m} and h_{m}, i.e. the values of ψ_{m} and h_{m} at time t^{n+1}, violated either of the two inequalities

$$\psi_{\mathrm{m}} - h_{\mathrm{m}} \leqslant \psi_{\mathrm{m}}^n \leqslant \psi_{\mathrm{m}} + h_{\mathrm{m}} \tag{31}$$

$$h_{\mathrm{m}}^n/2 \leqslant h_{\mathrm{m}} \leqslant 2h_{\mathrm{m}}^n \tag{32}$$

If one of the criteria defined by equations (31) and (32) is violated in the calculations, the grid has to be redefined. A method is required to calculate the values of the dependent variables in the new grid based upon the values obtained in the old (previous) grid. This can be achieved in several ways such as interpolation or projection methods. In the calculations reported here, the solution variables, i.e. the values of T, Y_1 and Y_2, were mapped onto the new mesh using the projection method developed by Lee and Ramos.[8]

Assume that the solution at time $t^n = n\Delta t$ is known and given by

$$A^n(t, \psi) = \sum_{j=1}^{\mathrm{NE}+1} a_j^n(t)\phi_j^n(\psi) \tag{33}$$

where a_j is the nodal amplitude and ϕ_j are the finite element basis which, in the calculations reported here, are the standard roof functions. Suppose also that at this time the mesh has to be redefined. Evidently, the values of the nodal amplitudes at time t^n in the new grid are needed because these values are the initial conditions for the next time step. Suppose then that $\phi_j^{n+1}(\psi)$ are the new finite element basis. We then define the initial conditions in the new grid as

$$A^* = \sum_{l=1}^{\mathrm{NE}+1} b_l^n(t)\phi_l^{n+1}(\psi) \tag{34}$$

and the functional

$$I = \tfrac{1}{2}(A^*, A^*) - (A^n, A^*) \tag{35}$$

where the inner product is given by

$$(A^n, A^*) = \int_0^{\psi_T} A^n A^* \, d\psi \tag{36}$$

The minimization of I yields the values of the nodal amplitudes, $b_i^n(t)$, in the new grid.

So far we have defined the criteria for grid location and redefinition, but we have not indicated the solution method for equation (14). In the calculations reported here we have employed a finite element algorithm which makes use of linear basis, i.e. the standard roof functions, as follows. Equation (14) is multiplied by ϕ_j and integrated by parts, to yield, after substituting

$$A(t, \psi) = \sum_{i=1}^{NE+1} q_i(t)\phi_i(\psi) \tag{37}$$

the following equation

$$\sum_{i=1}^{NE+1} (M_{ij}\dot{q}_i + aK_{ij}q_i) = \int_0^{\psi_T} S\phi_j \, d\psi \tag{38}$$

where

$$M_{ij} = \int_0^{\psi_T} \phi_i \phi_j \, d\psi \tag{39}$$

$$K_{ij} = \int_0^{\psi_T} \frac{\partial \phi_i}{\partial \psi} \frac{\partial \phi_j}{\partial \psi} d\psi \tag{40}$$

Equation (38) represents a system of ordinary differential equations for the nodal amplitudes $q_i(t)$. These differential equations were discretized at t^{n+1} to yield the following system of algebraic equations

$$\sum_{i=1}^{NE+1} \left[M_{ij} \frac{q_i^{n+1} - q_i^n}{\Delta t} + \alpha K_{ij} q_i^n \right] = \int_0^{\psi_T} S^{n+1} \phi_j \, d\psi \tag{41}$$

which were solved iteratively until the following convergence criterion was reached

$$\sum_{i=1}^{NE+1} \sqrt{[|(A_i^2)^{k+1} - (A_i^2)^k|]}/(NE+1) \leqslant 10^{-4} \tag{42}$$

where k denotes iteration.

PRESENTATION OF RESULTS

The calculations reported here were performed with 36 elements. Some representative results are shown in Figures 1–10. These results were computed with a time step equal to 1 μs which is about 60 times smaller than the time employed in the non-dimensionalization of the equations.

Figures 1–5 show the temperature and species mass fraction profiles at different times as a function of ψ/ψ_0, and Figures 5–10 show the temperature and species mass fraction profiles at different times as a function of the non-dimensional cartesian co-ordinate X (cf. equation (22)). These Figures show the early development of the flame, the diffusion of heat and the approach to the final steady state values. The flame speeds given by equation (24) differ from each other by less than 0·05 per cent and correspond to a value of 49·75 cm/s at a time equal to 2057 μs. This flame speed is in very good agreement with those calculated by Margolis,[2] Reitz[4] and Ramos.[5] For convenience the results of this and previous studies are shown in Table I. It can be seen from this Table that the adaptive finite element method developed in this paper is in very good agreement

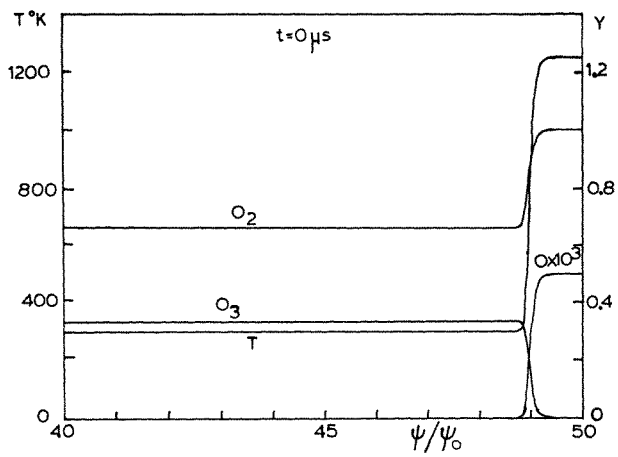

Figure 1. Temperature and species mass fraction profiles at time $t = 0$s as a function of ψ/ψ_0

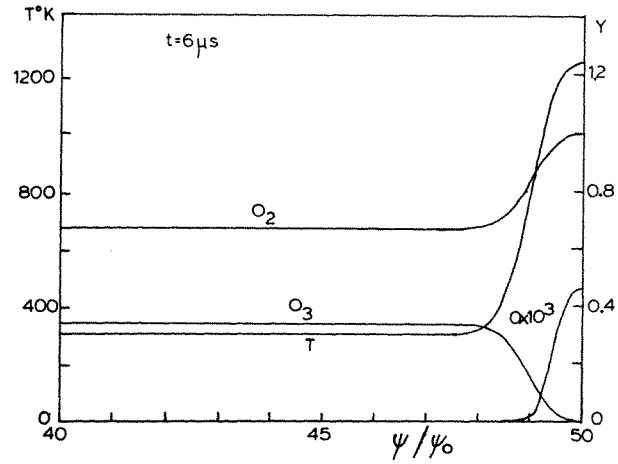

Figure 2. Temperature and species mass fraction profiles at time $t = 6\,\mu$s as a function of ψ/ψ_0

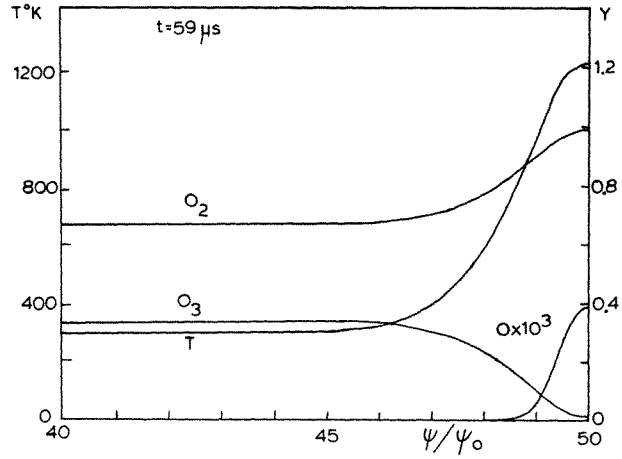

Figure 3. Temperature and species mass fraction profiles at time $t = 59\,\mu$s as a function of ψ/ψ_0

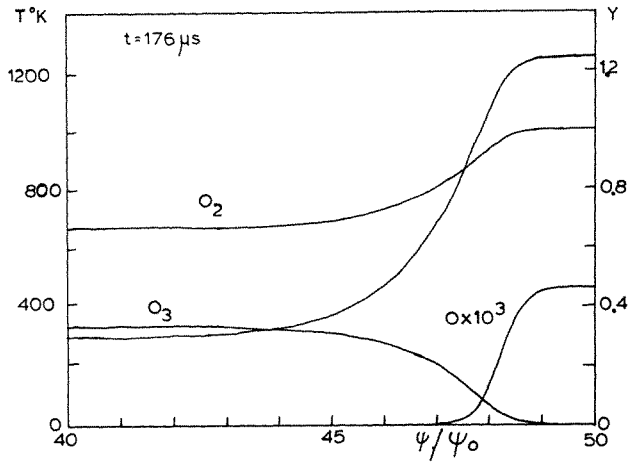

Figure 4. Temperature and species mass fraction profiles at time $t = 176\,\mu$s as a function of ψ/ψ_0

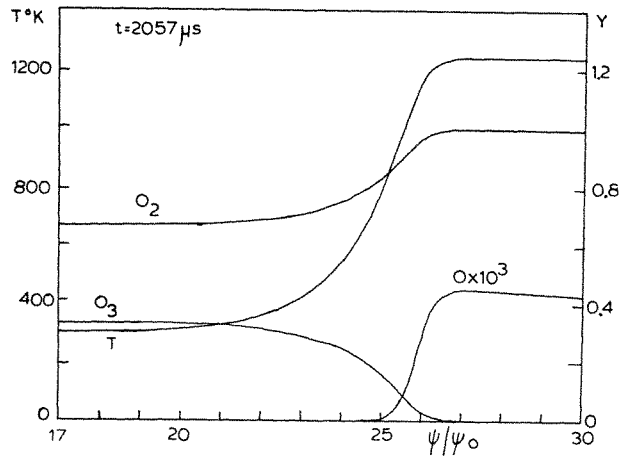

Figure 5. Temperature and species mass fraction profiles at time $t = 2057\,\mu$s as a function of ψ/ψ_0

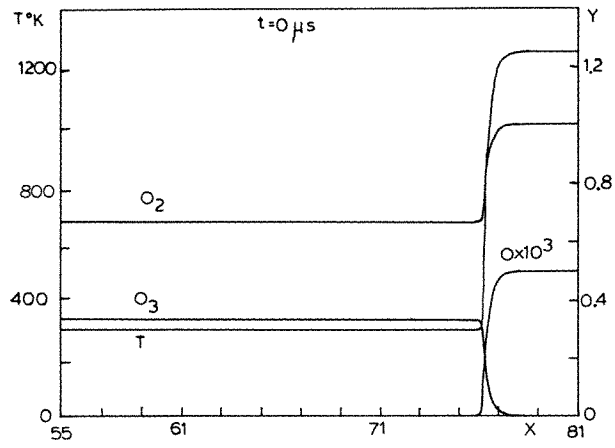

Figure 6. Temperature and species mass fraction profiles at time $t = 0$ s as a function of X

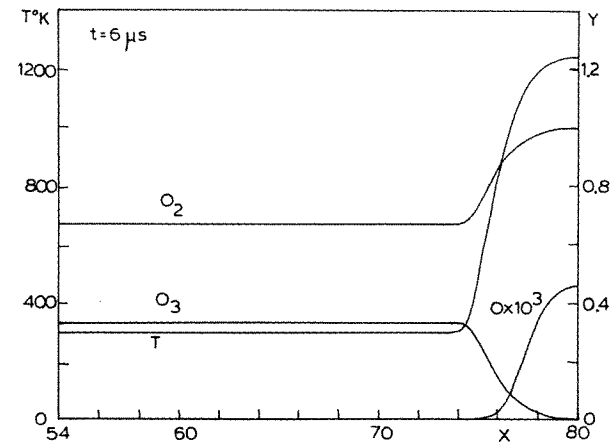

Figure 7. Temperature and species mass fraction profiles at time $t = 6\ \mu$s as a function of X

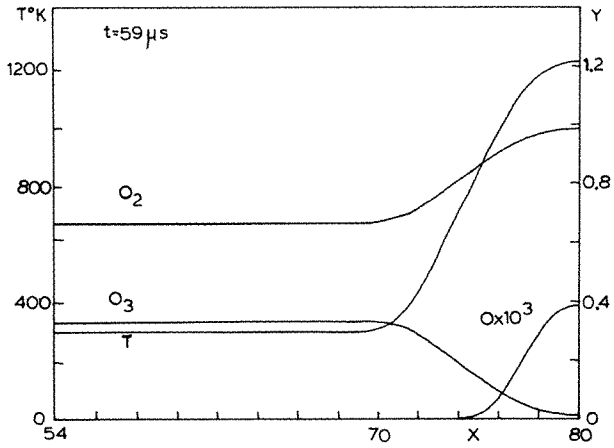

Figure 8. Temperature and species mass fraction profiles at time $t = 59\ \mu$s as a function of X

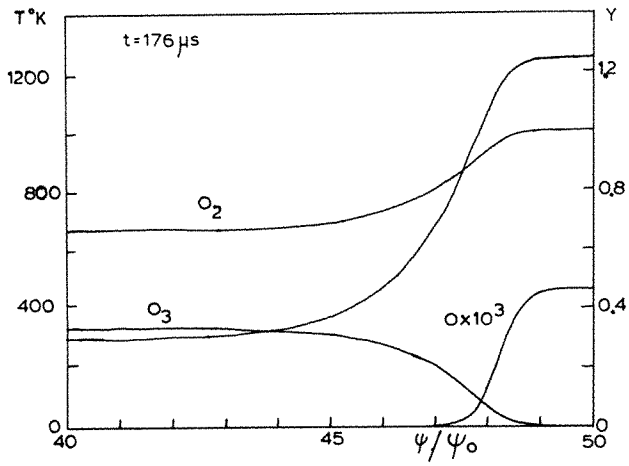

Figure 9. Temperature and species mass fraction profiles at time $t = 176\ \mu$s as a function of X

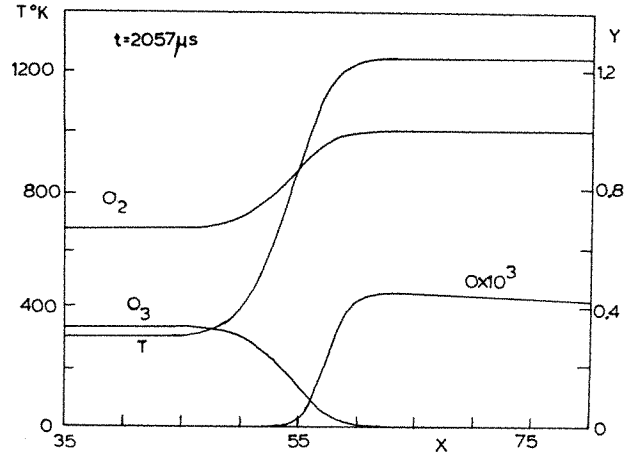

Figure 10. Temperature and species mass fraction profiles at time $t = 2057\ \mu$s as a function of X

Table I. Comparison of the ozone decomposition steady state flame speed

Investigator	Reference	Numerical method	Number of grid points	Steady state flame speed, cm/s
Bledjian	1	Second-order accurate method of lines	100	54.3
Margolis	2	Sixth-order B-splines	272 collocation points	49.7
Meintjes	3	Explicit predictor–corrector	121	48 ± 2
Reitz	4	Explicit, adaptive finite-difference	30	$49{\cdot}8 \pm 0{\cdot}1$
Ramos	5	Fourth-order accurate method of lines	121	49·57
Ramos	5	Fourth-order operator–splitting method	121	49·51
Ramos	5	First-order time-linearization	121	48·91
Ramos	5	Second-order time-linearization	121	48·97
Ramos	5	Fourth-order time-linearization	121	49·38
Ramos	5	Moving finite element method	36	49·26
Ramos	5	Adaptive finite element method	36	49·41
Ramos	This work	Adaptive finite element method	36	49·76

with the adaptive finite-difference scheme of Reitz[4] and the adaptive and moving finite element methods of Ramos.[5] The steady flame speeds are also in very good agreement with the more accurate, fixed-node technique of Margolis[2] and the fourth-order accurate method of lines and operator-splitting technique of Ramos.[5]

The main difference between the results presented here and those of Margolis[2] appear in the atomic oxygen profile. Our calculations indicate that the atomic oxygen decreases slightly slower than that computed by Margolis.[2] The results, however, are in very good agreement with those reported by Reitz[4] and Ramos.[5]

The numerical results presented here indicate that very accurate temperature and species mass fraction profiles, and flame speeds can be obtained with adaptive finite element methods since these methods concentrate most of the elements at the flame front where the largest temperature and species mass fraction gradients occur. They also indicate that the simplest finite element basis can yield results as accurate as fixed-node, fourth-order accurate finite-difference techniques while using a smaller number of nodes.

CONCLUSIONS

An adaptive finite element method has been developed and applied to study the ozone decomposition laminar flame. The method uses a fixed number of elements and a semidiscrete, linear Galerkin approximation. The nodes and size of the elements are moved according to the location of the largest temperature gradient in such a way that the mesh spacing is minimized. A criterion for mesh redefinition based on a projection method has also been introduced.

The system of ordinary differential equations which govern the nodal amplitudes was solved iteratively, and the non-linear reaction terms were linearized. The calculations show that the finite element results reported here are in very good agreement with those computed using fourth-order accurate, fixed-node finite–difference techniques. This is because the nodes and elements are concentrated at the flame front where the largest temperature and species mass fraction gradients occur. However, the adaptive finite element method presented here employs a fixed number of elements and a parabolic grid spacing. Although this mesh spacing shows some advantanges for the problem treated here, it is still crude and can be easily improved on. In addition, the adaptive method developed in this paper cannot deal in its present form with problems characterized by the presence of multiple moving fronts.

In spite of the accuracy and efficiency of the adaptive finite element technique developed in this paper, much more work is needed to assess its potential and to determine error estimates in problems characterized by the presence of moving fronts.

REFERENCES

1. L. Bledjian, 'Computation of time-dependent laminar flame structure', *Combustion and Flame*, **20**, 5–17 (1973).
2. S. B. Margolis, 'Time-dependent solution of a premixed laminar flame', *Journal of Computational Physics*, **27**, 410–427 (1978).
3. K. Meintjes, 'Predictor-corrector methods for time dependent compressible flows', *Ph.D. Thesis*, Princeton University, Princeton, New Jersey, 1979.
4. R. D. Reitz, *The Application of an Explicit Numerical Method to a Reaction–Diffusion System in Combustion*, The Courant Institute of Mathematical Sciences, New York University, New York, 1979.
5. J. I. Ramos, 'The application of finite-difference and finite element methods to a reaction-diffusion system in combustion', in C. Taylor, J. A. Johnson and W. R. Smith (eds), *Numerical Methods in Laminar and Turbulent Flow*, Pineridge Press, Swansea, U.K., 1983, pp. 1137–1147.
6. V. K. Saul'yev, *Integration of Equations of Parabolic Type by the Method of Nets*, Pergamon Press, New York, 1964.
7. P. J. Roache, *Computational Fluid Dynamics*, Hermosa Publishers, Albuquerque, New Mexico, 1976.
8. D. N. Lee and J. I. Ramos, 'Application of the finite-element method to one-dimensional flame propagation problems', *AIAA Journal*, **21**, 262–269 (1983).